1714 *Biochemistry* **2011,** *50,* 1714–1722
DOI: 10.1021/bi101575u

BIOCHEMISTRY
including biophysical chemistry & molecular biology
Article

Thermodynamic Analysis of Interactions between Cofactor and Neuronal Nitric Oxide Synthase[†]

Ryuhei Sanae, Fumiaki Kurokawa, Masayuki Oda, Sumio Ishijima, and Ikuko Sagami*

Graduate School of Life and Environmental Sciences, Kyoto Prefectural University, Shimogamo, Sakyo-ku, Kyoto 606-8522, Japan

Received October 22, 2010; Revised Manuscript Received January 11, 2011

ABSTRACT: The thermodynamics of cofactor binding to the isolated reductase domain (Red) of nNOS and its mutants have been studied by isothermal titration calorimetry. The $NADP^+$ and 2′,5′-ADP binding stoichiometry to Red were both 1:1, consistent with a one-site kinetic model instead of a two-site model. The binding constant (K_D = 71 nM) and the large heat capacity change ($\Delta C_p = -440$ cal mol^{-1} K^{-1}) for 2′,5′-ADP were remarkably different from those for $NADP^+$ (1.7 μM and −140 cal mol^{-1} K^{-1}, respectively). These results indicate that the nicotinamide moiety as well as the adenosine moiety has an important role in binding to nNOS. They also suggest that the thermodynamics of the conformational change in Red caused by cofactor binding are significantly different from the conformational changes that occur in cytochrome *c* reductase, in which the nicotinamide moiety of the cofactor is not essential for binding. Analysis of the deletion mutant of the autoinhibitory helix (RedΔ40) revealed that the deletion resulted in a decrease in the binding affinity of 2′,5′-ADP with more unfavorable enthalpy gain. In the case of RedCaM, which contains a calmodulin (CaM) binding site, the presence of Ca^{2+}/CaM caused a 6.7-fold increase in the binding affinity for 2′,5′-ADP that was mostly due to the favorable entropy change. These results are consistent with a model in which Ca^{2+}/CaM induces a conformational change in NOS to a flexible "open" form from a "closed" form that locked by cofactor binding, and this change facilitates the electron transfer required for catalysis.

Nitric oxide (NO) plays a crucial role as a signaling molecule in key physiological processes, such as neurotransmission, blood pressure regulation, and the immune response (*1*, *2*). Because of its diverse physiological effects, the NO synthesis pathway that is mediated by the nitric oxide synthases (NOSs)[1] is highly regulated by complex mechanisms. NOSs catalyze the formation of NO and L-citrulline from L-arginine in an oxidative process requiring NADPH and molecular oxygen. In mammals, the activities of the two constitutively expressed NOS isozymes, endothelial NOS (eNOS) and neuronal NOS (nNOS), are regulated by intracellular Ca^{2+} concentration via the reversible binding of calmodulin (CaM) (*3*, *4*). Conversely, the activity of inducible NOS (iNOS) is independent of changes in cellular Ca^{2+} concentrations because CaM always binds to iNOS at the basal level of Ca^{2+} in the cell, and the regulation of activity occurs primarily through transcriptional processes.

Each NOS isoform is homodimeric with subunits that consist of an N-terminal catalytic oxygenase domain and a C-terminal electron-supplying reductase domain (Red) linked by a Ca^{2+}/CaM binding site (Figure 1) (*5*, *6*). The oxygenase domain, in which NO synthesis takes place, contains a cysteine-ligated heme, a tetrahydrobiopterin (H_4B), and L-arginine (*5*−*8*). The reductase domain contains FMN, FAD, and NADPH-binding domains and belongs to a large protein family that includes cytochrome P450 reductase (CPR), sulfite reductase flavoprotein, and methionine synthase reductase (*9*−*12*). The crystal structure of rat nNOS Red indicates that there is a conserved organization of FMN, FAD, and NADPH-binding domains that is shared with CPR (*9*, *10*). Among these dual-flavin enzymes, NOS has a number of unique features. In NOS dimer, electrons derived from NADPH are sequentially transferred from FAD to FMN within the reductase domain of one subunit, and the electrons are then transferred to the heme in the oxygenase domain of the other subunit, which is accompanied by a large-scale conformational change (*13*, *14*). Ca^{2+}/CaM binding to NOS triggers this electron transfer for NO formation. Ca^{2+}/CaM also accelerates NADPH-dependent flavin reductions and transfer of electrons to external electron acceptors, such as cytochrome *c*, in the isolated NOS reductase domain containing the CaM binding site (RedCaM) (*15*, *16*). In addition to CaM binding, two control elements in the NOS reductase domain are involved in the regulation of electron transfer. One element is an autoinhibitory helix insert (AH) of approximately 40 amino acids in the FMN-binding domain of nNOS and eNOS that is not found in iNOS and CPR. The other element is an extension of the C-terminus (CT); all NOS isoforms are 20−40 residues longer than CPR. Deletion of either the AH or CT results in activation of electron transfer in CaM-free RedCaM and NO formation in the holoenzyme even in the absence of Ca^{2+}/CaM, which demonstrates that each of these elements acts as an autoinihibitory domain for NO formation under conditions of low Ca^{2+} concentration (*17*−*22*).

[†]This study was in part supported by Grants-in-Aid from the Ministry of Education, Culture, Sports, Science, and Technology of Japan to I.S. (20570139).

*To whom correspondence should be addressed. Phone: +81-75-703-5672. Fax: +81-75-703-5672. E-mail: sagami@kpu.ac.jp.

[1]Abbreviations: 2′,5′-ADP, adenosine 2′,5′-diphosphate; CaM, calmodulin; C_p, heat capacity; CPR, cytochrome P450 reductase; FAD, flavin adenine dinucleotide; FMN, flavin mononucleotide; H_4B, tetrahydrobiopterin; ITC, isothermal titration calorimetry; NOS, nitric oxide synthase; Red, reductase domain of nNOS; RedCaM, reductase domain including the Ca^{2+}/CaM binding site of nNOS; cyt *c*, cytochrome *c*; IPTG, isopropyl 1-β-thiogalactoside; PMSF, phenylmethanesulfonyl fluoride.

 Published on Web 01/18/2011

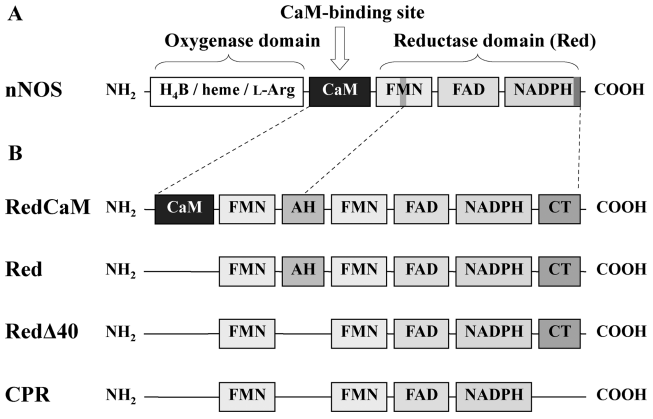

FIGURE 1: Domain structures of nNOS and its mutants. (A) Domain organization of full-length nNOS. The schematic representation shows the domain organization of nNOS. (B) The domain structures of nNOS Red and its mutants. All of the reductases except for CPR were used in this study. The 40 amino acids of the autoinhibitory domain within the FMN subdomain are deleted in the Δ40 mutant. Red and RedCaM refer to the isolated reductase domain with and without the CaM binding domain, respectively.

Phosphorylation at sites in the autoinhibitory domains has also been shown to affect Ca^{2+} sensitivity and electron transfer for NO formation in eNOS and nNOS (*23*−*25*).

NADPH binding is also important for regulating electron transfer in nNOS (*26*, *27*). The binding of NADPH to CaM-free RedCaM inhibits electron transfer to cytochrome *c*, suggesting that the CaM-free enzyme with NADPH forms a conformationally "closed" complex. In the closed complex, the FMN subdomain is shielded within the enzyme dimer interface, resulting in the suppression of electron transfer. The binding of Ca^{2+}/CaM to nNOS is thought to induce a conformational rearrangement that facilitates electron transfer by releasing a NADPH-dependent conformational lock. In the crystal structure with $NADP^+$, both of the AH and CT regulatory domains are located between the FMN-, FAD-, and NADPH-binding domains, and consequently, FMN is buried, which supports the closed model induced by NADPH binding. Combined with the crystal structure, mutagenesis studies support this unique mechanism in which the AH and CT domains, in addition to NADPH binding, synergistically repress NOS activity by locking the FMN binding domain into an electron-accepting position (FMN-shielded) (*28*−*34*). In this mechanism, CaM binding or phosphorylation of the AH or CT domains induces a large-scale swinging motion of the entire FMN domain to transfer the electrons required for the catalytic activity (FMN-deshielded). However, the precise mechanism for how NADPH binding induces the conformational change of the reductase domain is still unclear because there is a lack of sufficient structural information, e.g., the whole structure of the reductase domain with the CaM binding site and the structure without NADPH. There are also conflicting reports on the binding stoichiometry of the cofactor to the reductase domain of NOS. Knight and Scrutton (*35*) proposed that multiple molecules of cofactor bind to NOS based on stopped-flow kinetic studies, while other studies support a single-binding site model (*36*).

In this paper, to confirm the binding stoichiometry between NOS and its cofactor and the conformational change of nNOS reductase domain induced cofactor binding, we have performed thermodynamic studies using isothermal titration calorimetry (ITC) to examine the binding of cofactor to the isolated reductase domain of nNOS. These experiments were conducted without (Red) and with the CaM binding domain (RedCaM) and with the AH-deletion mutant (RedΔ40). ITC is a pure solution technique used to study interactions between a protein and its ligand, and this technique is a powerful tool for the direct measurement of thermodynamic parameters. We determined the Gibbs free energy (ΔG), enthalpy (ΔH), and entropy (ΔS) changes as well as the association constant (K_a) and the number of binding sites (n) for 2′,5′-ADP and $NADP^+$ in the nNOS reductases and compared these values with those of CPR (*37*). The thermodynamic parameters reported here reveal the difference in cofactor-binding character between the nNOS Red and CPR. Our studies also demonstrate that both the CaM binding site and the AH domain actually modulate the interaction between the reductase domain of nNOS and its cofactor.

EXPERIMENTAL PROCEDURES

Materials. 2′,5′-ADP Sepharose 4B and Sephadex G-25 medium were purchased from GE Healthcare U.K. Ltd. (Buckinghamshire, England). TOYOPEARL DEAE-650 M was obtained from TOSOH Co., Ltd. (Tokyo, Japan). 2′,5′-ADP and $NADP^+$ were purchased from Sigma-Aldrich Japan K.K. (Tokyo, Japan). Aprotinin, leupeptin, and pepstatin A were purchased from Peptide Institute, Inc. (Osaka, Japan). All other reagents were of the best analytical grade available and were obtained from Wako Pure Chemical Industries, Ltd. (Osaka, Japan), or Nacalai Tesque, Inc. (Kyoto, Japan).

Plasmids. pCRNNR for coexpression of the rat nNOS reductase domain with the CaM binding site (designated RedCaM, residues 695−1429) and the bovine brain CaM were provided by Dr. S. Daff (University of Edinburgh, U.K.) (*21*). Expression plasmids for the rat nNOS reductase domain without the CaM binding site (Red, residues 746−1429) and the reductase domain without the autoinhibitory helix region (RedΔ40, residues 746−831/870−1429) were constructed in pCWori$^+$ and pET-28a(+), respectively, as described previously (*38*, *39*). The plasmid pGroESL, which was used for the production of *Escherichia coli* chaperones, was a gift from DuPont de Nemours and Co. (Wilmington, DE) (*40*).

Expression and Purification of nNOS Red, RedΔ40, and RedCaM. Expression of nNOS Red, RedΔ40, and RedCaM was carried out using the plasmids Red/pCWori$^+$, RedΔ40/pET-28a(+), and pCRNNR, respectively, with coexpression of *E. coli* chaperones (pGroESL) in BL21 (DE3) cells. The culture was continued in LB containing 50 μg/mL ampicillin (for Red/pCWori$^+$ and pCRNNR) or 30 μg/mL kanamycin (for RedΔ40/pET-28a(+)) and 35 μg/mL chloramphenicol (for pGroESL) at 37 °C until the absorbance at 600 nm reached approximately 0.8, and then final concentrations of 3 μM riboflavin and 0.2 mM IPTG for pCRNNR or 0.5 mM IPTG for Red/pCWori$^+$ and RedΔ40/pET-28a(+) were added to induce the expression of the proteins. Cells were further cultured at 30 °C for 20 h for Red/pCWori$^+$ and RedΔ40/pET-28a(+) or 24 h for pCRNNR.

Proteins were purified by a modified method that has been previously described (*38*). To avoid the contamination of the cofactor before ITC measurements were performed, a high salt buffer was used instead of cofactor solution to elute the enzyme from a 2′,5′-ADP Sepharose 4B column. Briefly, the cell lysate was loaded onto a 1.5 × 5.5 cm column of 2′,5′-ADP Sepharose 4B equilibrated with buffer A (50 mM Tris-HCl, pH 7.5, at 25 °C, 50 mM NaCl, 10% glycerol, 1 mM DTT, 2 μg/mL aprotinin,

2 μg/mL leupeptin, 2 μg/mL pepstatin A). The column was washed with 100 mL of buffer A, and then nNOS Red or RedΔ40 was eluted with 50 mL of buffer A containing 1.5 M NaCl. The protein was precipitated by adding ammonium sulfate to 60% saturation. The ammonium sulfate precipitate was collected by centrifugation and dissolved in 10 mL of buffer A; this solution was loaded onto a 3 × 5 cm column of Sephadex G-25 medium equilibrated with buffer B (50 mM Tris-HCl, pH 7.5, at 25 °C, 10% glycerol, 1 mM DTT). The protein fractions were pooled and sequentially loaded onto a 2 × 5 cm column of TOYOPEARL DEAE-650 M equilibrated with buffer B. After being washed with 100 mL of buffer B, nNOS Red or RedΔ40 was eluted with buffer B containing 150 mM NaCl. The purified protein was passed through a 3 × 5 cm column of Sephadex G-25 medium equilibrated with ITC buffer (100 mM Bes−NaOH, pH 7.0, at the ITC measurement temperature, with or without 10% glycerol). The protein fractions were collected and filtered through a 0.2 μm filter, DISMIC-25CS (Toyo Roshi, Ltd., Tokyo, Japan), for ITC measurements. The filtered enzyme was quickly frozen with liquid nitrogen and stored at −80 °C.

For purification of nNOS RedCaM, buffer C (50 mM Tris-HCl, pH 7.5, at 25 °C, 50 mM NaCl, 10% glycerol, 1 mM DTT, 5 mM $CaCl_2$, 1 mM EDTA, 2 μg/mL aprotinin, 2 μg/mL leupeptin, 2 μg/mL pepstatin A, 1 mM freshly prepared PMSF) containing 10 μM FAD and 10 μM FMN and buffer D (50 mM Tris-HCl, pH 7.5, at 25 °C, 10% glycerol, 1 mM DTT, 0.5 mM $CaCl_2$) were used instead of buffers A and B, respectively. In TOYOPEARL DEAE-650 M chromatography, after two washing steps with 100 mL of buffer D and 20 mL of buffer D containing 75 mM NaCl, nNOS RedCaM with Ca^{2+}/CaM was eluted with buffer D containing 150 mM NaCl. The purified RedCaM with Ca^{2+}/CaM was concentrated to 30 μM using an Ultra Filter Unit USY-5 (Toyo Roshi, Ltd., Tokyo, Japan). The purified protein was passed through a 3 × 5 cm column of Sephadex G-25 medium equilibrated with the ITC buffer containing 0.5 mM $CaCl_2$.

To prepare nNOS RedCaM without CaM, the RedCaM protein eluted from the TOYOPEARL DEAE-650 M column was then loaded onto a 1.5 × 5.5 cm column of 2′,5′-ADP Sepharose 4B equilibrated with buffer E (50 mM Tris-HCl, pH 7.5, at 25 °C, 10% glycerol, 1 mM DTT, 5 mM EGTA). The column was washed with 50 mL of buffer E, and then nNOS RedCaM without Ca^{2+}/CaM was eluted with 50 mL of buffer E containing 1.5 M NaCl. After 60% ammonium sulfate precipitation, the enzyme solution was passed through a 3 × 5 cm column of Sephadex G-25 medium equilibrated with the ITC buffer.

RedCaM with or without CaM, Red, and RedΔ40 were purified to more than 90% purity as determined by SDS−PAGE (Supporting Information Figure S1).

Determination of Enzyme Concentration. The enzyme concentrations were determined by measuring the flavin content spectrophotometrically. The absorption spectra (250−700 nm) of the enzymes were measured at 25 °C using a UV−visible UV-1800 spectrophotometer (Shimadzu, Japan). A volume of 0.5 μL of 1 mM potassium ferricyanide, a one-electron acceptor, was added to 100 μL of the protein solution. After a 1 min incubation, the spectra were measured, and this procedure was repeated a total of 10 times. Nearly all of the enzymes prepared in this study showed little change in the absorbance at 457 nm after addition of potassium ferricyanide, indicating that the enzymes were mostly oxidized during purification (Supporting Information Figure S2). Enzyme concentrations were calculated from the absorbance at 457 nm of the fully oxidized nNOS reductase domain using a molar extinction coefficient of 22.9 $mM^{-1}\cdot cm^{-1}$. The protein concentrations were also determined by the Bradford method. The FMN and FAD contents relative to the protein content for each enzyme were found to be between 0.9 and 0.8.

Catalytic Activity of Purified Enzyme. The activity of nNOS Red and its mutants was characterized by the reduction of the exogenous electron acceptor cytochrome *c* as described previously (*21*). The final concentrations in the reaction mixture consisted of 10 mM HEPES−NaOH, pH 7.0, at 25 °C, 5 μM FAD, 5 μM FMN, 0.5 mM $CaCl_2$, 100 μM cytochrome *c* (from horse heart), and an appropriate concentration of the NOS enzyme. The mixture was preincubated at 25 °C for 5 min, and the reaction was initiated by the addition of NADPH at a final concentration of 200 μM. The cytochrome *c* reduction activity was calculated from the absorbance at 550 nm over time using a molar extinction coefficient of 21 $mM^{-1}\cdot cm^{-1}$. The reactions were performed in triplicate.

Isothermal Titration Calorimetry (ITC) Measurements. ITC experiments were conducted for thermodynamic analyses of the interactions between the oxidized Red of nNOS and its mutants with 2′,5′-ADP and $NADP^+$ using a MCS-ITC (MicroCal Inc., Northampton, MA). Purified enzymes and NADPH analogues for the microcalorimetry measurements were dissolved in ITC buffer (100 mM Bes−NaOH, pH 7.0, at the experimental temperature, with or without 10% glycerol). Concentrations of 2′,5′-ADP and $NADP^+$ were calculated using the molar extinction coefficients of 15.4 $mM^{-1}\cdot cm^{-1}$ and 18.0 $mM^{-1}\cdot cm^{-1}$, respectively, at 260 nm. All samples were degassed for 10 min before the titrations. 2′,5′-ADP or $NADP^+$ was titrated into nNOS Red or its mutants, and each titration consisted of a small quantity of an initial injection followed by 20−30 main injections. Acquisition data were analyzed using MicroCal Origin Version 2.9 (MicroCal Software, Inc.). After subtracting the heat of ligand dilution, which was determined by injecting ligand into the same ITC buffer, the binding of ligand to nNOS Red and its mutants was quantified by fitting the evolved heat per injection to a single-site binding model using a nonlinear least-squares method. Except for the initial injection, fitting of the binding isotherm was carried out through multiple iterations until a minimum X^2 value was obtained. The reported values are an average of at least three ITC runs. The binding stoichiometry (*n*), the association constant (K_a), and the enthalpy change (ΔH) were obtained from the fitted curve. The values of the Gibbs free energy change (ΔG) and the entropy change (ΔS) were calculated from the equation:

$$\Delta G = -RT \ln K_a = \Delta H - T\Delta S$$

where *R* is the gas constant and *T* is the absolute temperature. In line with common usage in the enzyme kinetics literature, the dissociation constant K_d is also used in the text ($K_d = 1/K_a$). The temperature dependence studies were performed over the range from 15 to 30 °C. The heat capacity change, ΔC_p, was calculated from the linear fitting of the ΔH values measured at various experimental temperatures.

After the ITC measurements, each of the samples was collected and applied to a Bio-Spin 6 column (Bio-Rad Laboratories, Inc., Hercules, CA) equilibrated in 10 mM HEPES buffer, pH 7.0, at 25 °C, with 10% glycerol to remove NADPH analogues. The residual activity was then analyzed to determine the stability of the protein.

Table 1: Reduction of Cytochrome *c* by the Isolated nNOS Reductase Domains

	cytochrome *c* reduction[a] (μmol min^{-1} μmol^{-1})	K_m for NADPH (μM)	K_a for NADPH[b] ($\times 10^4$ M^{-1})
Red	152 ± 28	2.1 ± 0.2	48
RedΔ40	702 ± 98	0.9 ± 0.2	110
RedCaM with CaM[c]	2860 ± 320	2.3 ± 0.2	43
RedCaM without CaM	288 ± 63	1.7 ± 0.1	59

[a] k_{cat} values were determined as described in the Experimental Procedures at 25 °C and expressed as moles of reduced cytochrome *c* per mole of enzyme per minute. The mean and standard deviation for three to five independently purified enzymes are represented. [b] K_a values were calculated from K_m ($K_a = 1/K_m$). [c] k_{cat} value was determined in the presence of Ca^{2+} (0.5 mM).

RESULTS AND DISCUSSION

Catalytic Activities of Purified Enzymes. The activities of the purified enzymes were determined for the reduction of cytochrome *c* (Table 1). The reduction rate (k_{cat}) of Red (152 μmol min^{-1} μmol^{-1}) for this reaction was similar to that of RedCaM in the absence of Ca^{2+}/CaM (288 μmol min^{-1} μmol^{-1}). The addition of Ca^{2+}/CaM to RedCaM increased the activity approximately 10-fold (2860 μmol min^{-1} μmol^{-1}) as described previously (*19*, *22*). RedΔ40, a deletion mutant lacking the AH insert, showed significant activity (702 μmol min^{-1} μmol^{-1}), even in the absence of the CaM binding site, indicating that the AH domain has an inhibitory role for electron transfer in the reductase domain under low Ca^{2+} concentration. Conversely, the K_m value for NADPH was not significantly affected by the CaM binding site in the presence or absence of CaM (K_m = ~2 μM). These K_m values are comparable to those that have been previously determined in another study (*19*). The K_m value for RedΔ40 was 0.9 μM, indicating that RedΔ40 has a higher affinity for NADPH. The K_a values for NADPH calculated from the K_m values ($K_a = 1/K_m$) are summarized in Table 1. To further elucidate the binding mechanism of cofactors to Red and its mutants, we used calorimetry to determine binding affinities and thermodynamic parameters for these enzymes. The catalytic activity of each reductase remained the same before and after each ITC measurement, confirming that the enzyme was stable during the measurements.

Binding Stoichiometry and Thermodynamic Parameters for Cofactor Binding to Red. Binding isotherms for the interaction of Red and $NADP^+$ or 2′,5′-ADP were obtained in 100 mM Bes−NaOH, pH 7.0, at 25 °C. A typical calorimetric titration with $NADP^+$ and 2′,5′-ADP is shown in panels A and B of Figure 2, respectively. The exothermic reaction was observed, and after subtracting dilution heat, the obtained heat data were described well by a one-set-of-sites model. In all of the experiments, the calculated binding stoichiometry (*n*) was 1 (Table 2), indicating that a single $NADP^+$ or 2′,5′-ADP molecule binds to each nNOS reductase molecule. Previously, a two-site binding model, in which two cofactor molecules bind to the catalytic and regulatory sites, has been proposed for CPR (*41*), BM3 (*42*), and NOS (*35*) based on pre-steady-state kinetic studies by Scrutton and co-workers. However, a two-site binding model remains controversial because only one bound $NADP^+$ molecule is shown in the crystal structures of the reductase domain of NOS (*8*, *9*) and CPR (*10*) (Figure 3). In addition, Daff has proposed an alternative one-binding-site model for the binding of

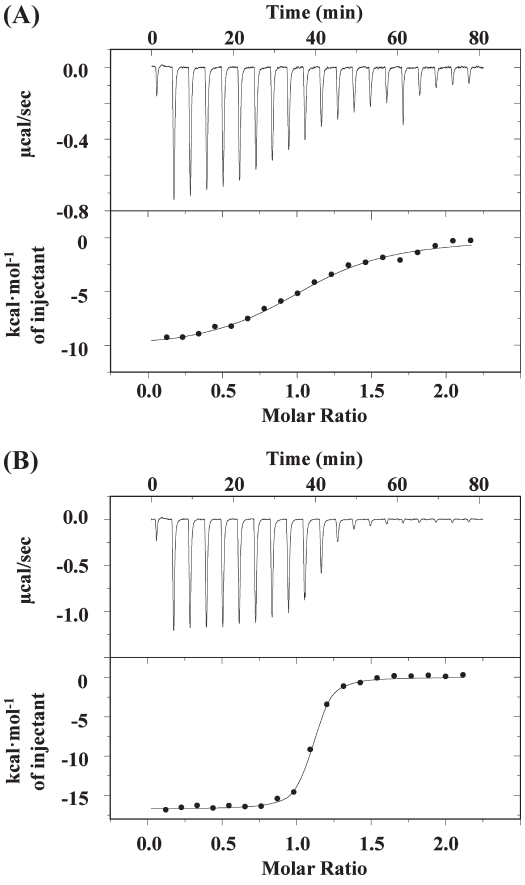

FIGURE 2: Interaction of Red with $NADP^+$ (A) and 2′,5′-ADP (B) at 25 °C in 100 mM Bes−NaOH, pH 7.0. Typical calorimetric titrations (upper panel) and the resulting integrated binding isotherms (lower panel) are shown. In these measurements, 9 μL aliquots of 0.263 mM $NADP^+$ (A) or 0.250 mM 2′,5′-ADP (B) were injected via syringe into 16.2 μM Red in the calorimetric cell, and the data were collected for a total of 20 injections at 4 min intervals. The first injection included only 2 μL of ligand, and the corresponding data point was deleted from the analysis. After subtracting the heat of ligand dilution from the reaction heat by performing the control experiment, the solid line connecting the integrated data points (lower panel) was obtained from a one-set-of-sites model fitting using a nonlinear least-squares method.

cofactor to these enzymes by reanalyzing the kinetic data (*36*). The data obtained here indicate that 2′,5′-ADP and $NADP^+$ also bind to nNOS with 1:1 stoichiometry. Thus, this thermodynamic analysis verified the single-binding-site model instead of a multiple-site model for NOS. In addition, a calorimetry study of cofactor binding to CPR was recently reported that also supports the one-binding-site model (*37*).

The thermodynamic parameters and the association constant of $NADP^+$ and 2′,5′-ADP binding to Red at 25 °C are summarized in Table 2 along with the data for CPR obtained by the other group under the same buffer conditions (*37*). The Gibbs free energy change (ΔG) of $NADP^+$ binding to Red (−7.8 kcal·mol^{-1}), which is directly related to the association constant (K_a), was larger than that of 2′,5′-ADP binding to Red (−9.8 kcal·mol^{-1}). As a consequence, the K_a value of $NADP^+$ binding to Red (58.2 × 10^4 M^{-1}) was much smaller than that of 2′,5′-ADP binding (1410 × 10^4 M^{-1}). The contributions of enthalpy (ΔH) and entropy ($T\Delta S$) changes to ΔG significantly differ for each cofactor. In contrast to 2′,5′-ADP binding to Red, an unfavorable large gain of ΔH contributed to the marked increase in the value of ΔG for binding of $NADP^+$ to Red despite a much

Table 2: Thermodynamic Parameters for the Interaction of Red and CPR with $NADP^+$ or 2′,5′-ADP Phosphate Ligands at 25 °C

	ligand	n	K_a ($\times 10^4$ M^{-1})	ΔH (kcal·mol^{-1})	ΔG^c (kcal·mol^{-1})	$T\Delta S^c$ (kcal·mol^{-1})
Red[a]	$NADP^+$	1.0	58.2 ± 3.3	−11 ± 0.5	−7.8 ± 0.0	−3.0 ± 0.5
	2′,5′-ADP	1.1	1410 ± 540	−17 ± 1.2	−9.8 ± 0.2	−7.0 ± 1.1
CPR[b]	$NADP^+$	1.1	1820 ± 50	−17 ± 0.1	−9.9	−7.1
	2′,5′-ADP	1.0	1900 ± 60	−18 ± 2.0	−9.9	−8.1

[a]The thermodynamic parameters (n, K_a, ΔH) were determined by ITC measurement in buffer (100 mM Bes−NaOH, pH 7.0, at 25 °C). All measurements were performed in triplicate. [b]The thermodynamic parameters (n, K_a, ΔH) of CPR determined under the same conditions were reported previously by Grunau et al. (*37*). [c]ΔG and $T\Delta S$ values were calculated as described in the Experimental Procedures.

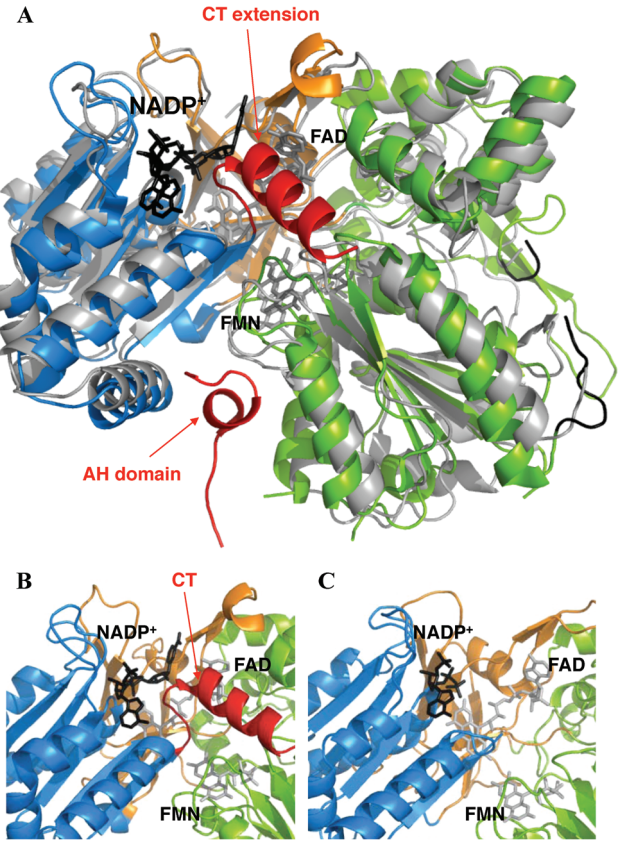

FIGURE 3: (A) The crystal structure of rat nNOS Red (PDB 1TLL) with a structural superposition of rat CPR (PDB 1AMO). (B, C) Comparison of the NADPH binding site of rat nNOS Red (B) with that of rat CPR (C). The different domains are colored in the crystal structures of rat NOS Red (PDB 1TLL) and rat CPR (PDB 1AMO) as follows: green, FMN-binding domain; orange, FAD-binding domain; blue, NADPH-binding domain; red, C-terminal extension (CT) and autoinhibitory helix (AH). Cofactors are shown as stick models with different colors: black, NADPH; gray, FMN and FAD.

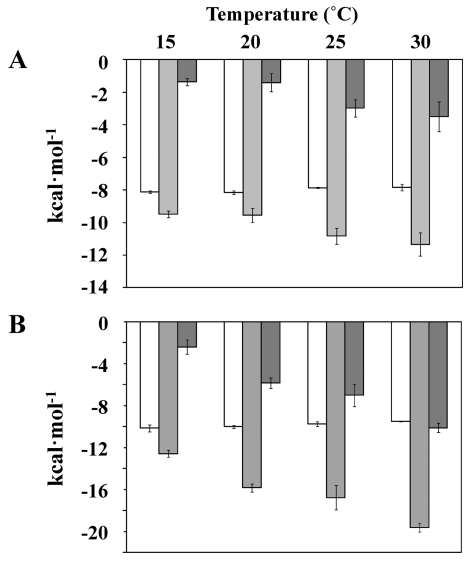

FIGURE 4: Comparison of thermodynamic parameters for the interaction between Red and $NADP^+$ (A) and 2′,5′-ADP (B) in 100 mM Bes−NaOH, pH 7.0, at the experimental temperature. The Gibbs free energy change for binding (ΔG) is represented in white, the enthalpy change for binding (ΔH) is represented in light gray, and the entropy change for binding ($T\Delta S$) is represented in dark gray. ITC measurements were performed in triplicate at each temperature, and the standard deviation is shown as a black line.

less unfavorable entropy change (Table 2). These results indicate that the nicotinamide moiety of $NADP^+$ significantly decreases the binding affinity to Red. Inhibition studies of NOS have demonstrated the primary importance of the adenosine moiety for coenzyme binding because 2′,5′-ADP is as effective as an inhibitor of electron transfer as $NADP^+$ (*43*, *44*). In addition, the electrochemical analysis of Red and the isolated FAD domain (residues 695−946) of nNOS revealed that $NADP^+$ binding stabilized the hydroquinone form of the FAD while ADP did not, suggesting that specific interactions occur between the nicotinamide moiety and the enzyme (*44*). In contrast, the K_a value of 2′,5′-ADP binding to Red is comparable to those of 2′,5′-ADP binding (1900×10^4 M^{-1}) and $NADP^+$ binding (1820×10^4 M^{-1}) to CPR. The similar K_a values for $NADP^+$ and 2′,5′-ADP binding to CPR are consistent with the essential role of the adenosine moiety for cofactor binding in the protein. In the crystal structure of the $NADP^+$ complex of rat CPR, the adenosine moiety bound to the enzyme through ionic interactions, hydrogen bonds, and hydrophobic stacking interactions while the nicotinamide moiety was thought to be solvent-exposed because of its flexibility (Figure 3C (*10*)). The crystal structure of Red shows that the nicotinamide moiety of $NADP^+$ is also solvent-exposed but ionically interacts with the residues of CT that are absent in CPR as shown in Figure 3B (*9*). While the AH domain is located rather far from the $NADP^+$ binding site, it is thought to control the conformational equilibrium of the reductase as mentioned later. Therefore, It is possible that these unique structural elements affect the binding of cofactor to Red. Taken together, these results indicate that the thermodynamics for $NADP^+$ and 2′,5′-ADP binding are different between NOS Red and CPR, although the overall structures of these proteins are very similar.

Temperature Dependence of the Thermodynamic Parameters for Red. To investigate the temperature dependence of the thermodynamic parameters in the binding of $NADP^+$ or 2′,5′-ADP to Red, the calorimetric titrations were carried out at 15, 20, 25, and 30 °C. As shown in Figure 4, the ΔG values for Red−cofactor complex formation were insensitive to temperature

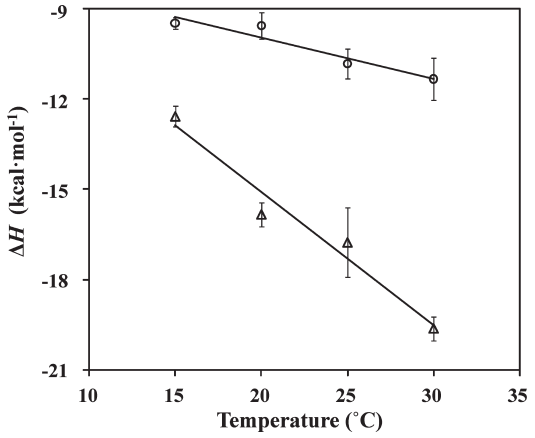

FIGURE 5: Temperature dependence of the observed ΔH values for $NADP^+$ and 2′,5′-ADP for Red in 100 mM Bes−NaOH, pH 7.0. The observed ΔH values were plotted versus temperature, and the ΔC_p value shown in Table 3 was obtained from its slope. Triangles, Red with 2′,5′-ADP; circles, Red with $NADP^+$. The fitted linear correlation coefficients (R^2) for Red with $NADP^+$ and with 2′,5′-ADP were 0.92 and 0.96, respectively.

Table 3: Heat Capacity Changes (ΔC_p) for the Binding Interaction of Red and CPR with NADPH Analogues

protein	ligand	ΔC_p (cal·mol^{-1}·K^{-1})
Red[a]	$NADP^+$	−140
Red[a]	2′,5′-ADP	−440
CPR[b]	$NADP^+$	−230
CPR[b]	2′,5′-ADP	−210

[a] ΔC_p values for Red were determined in 100 mM Bes−NaOH, pH 7.0, as described in the Experimental Procedures. [b] ΔC_p values for human CPR binding to $NADP^+$ and 2′,5′-ADP were recently reported by Grunau et al. (*37*).

due to the well-known compensatory effects of enthalpy and entropy, which are temperature dependent (*45*). The heat capacity change (ΔC_p) of the binding reaction was determined from the slope of the plot of ΔH versus temperature (Figure 5) and is summarized in Table 3. The ΔC_p for $NADP^+$ binding to Red (−140 cal·mol^{-1}·K^{-1}) was strikingly different from that for 2′,5′-ADP binding to Red (−440 cal·mol^{-1}·K^{-1}), while ΔC_p for $NADP^+$ binding to CPR was nearly the same as that for 2′,5′-ADP (approximately −220 cal·mol^{-1}·K^{-1}). The different ΔC_p values between Red and CPR again suggest that there are structural differences or different water networks for cofactor binding between these two proteins.

In protein−ligand interactions, negative heat capacity changes have been found to correlate to burial of the hydrophobic surface area (*46*−*49*). Water molecule networks in the protein−ligand interface were also suggested to contribute to a negative ΔC_p in addition to the burial of nonpolar surface area (*50*). Recently, Grunau and co-workers demonstrated an interplay between the thermodynamics of ligand binding to CPR and the induced conformational motion in the domain (*51*) . In a combination study using calorimetry and small-angle X-ray scattering, binding of 2′,5′-ADP to wild-type CPR was found to trigger a large-scale structural rearrangement that resulted in a more compact domain organization and a large decrease in the molecular diameter of the complex. Interestingly, a deletion mutant of CPR that was accompanied by a decrease in the number of thermodynamic microstates available to the ligand−CPR complex

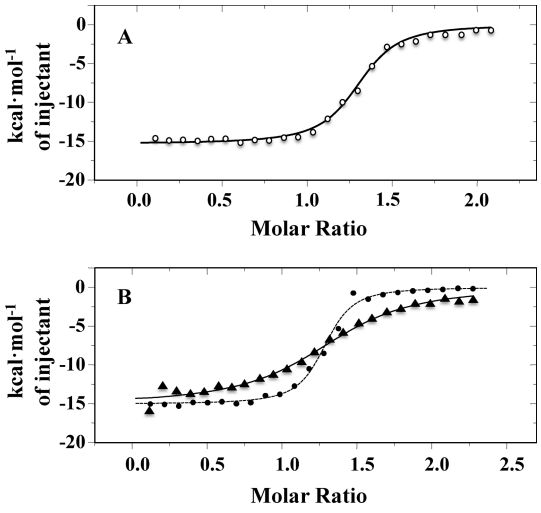

FIGURE 6: Interaction of RedΔ40 (A) and RedCaM (B) with 2′,5′-ADP at 20 °C. (A) Each 4 μL aliquot of 0.428 mM 2′,5′-ADP was injected into 15.0 μM RedΔ40. (B) Each 4 μL aliquot of 0.428 mM 2′,5′-ADP was injected into 13.9 μM RedCaM without CaM (▲) in 100 mM Bes−NaOH, pH 7.0, with 10% glycerol, and each 4 μL aliquot of 0.639 mM 2′,5′-ADP was injected into 19.9 μM RedCaM with CaM (●) in 100 mM Bes−NaOH, pH 7.0, with 10% glycerol and 0.5 mM $CaCl_2$. The data were collected for a total of 25 injections at 4 min intervals. The first injection included only 1 μL of ligand, and the corresponding data point was deleted from the analysis.

showed the most negative ΔC_p value (−580 cal·mol^{-1}·K^{-1}). These results suggest that the conformational constraints of the entire macromolecule would affect the negative ΔC_p value. Therefore, it is possible that the large, negative ΔC_p value for 2′,5′-ADP binding to Red is due to burial of significant nonpolar surface area and/or disruption of a hydrogen bond network in the vicinity of the binding site. Binding of 2′,5′-ADP to NOS Red may also induce restriction of the freedom of the entire macromolecule in comparison to the ligand−CPR complex. On the other hand, the less negative ΔC_p values for $NADP^+$ binding to Red indicate that the surface conditions and/or the water molecule network of Red are not significantly changed by cofactor binding. In any case, these results again imply that the nicotinamide moiety of the cofactor significantly affects the energy fluctuations in the Red−cofactor complex.

Effects of AH and CaM Binding Site on the Binding of 2′,5′-ADP. Interaction of RedΔ40, which contains a deletion of the AH insert, or RedCaM, which includes a CaM-binding site in Red with 2′,5′-ADP, was examined, and the data were compared with those of Red determined under the same conditions. RedΔ40 and RedCaM with or without CaM were less stable than Red. Therefore, ITC measurements were performed in ITC buffer containing 10% glycerol at 20 °C instead of 25 °C to maintain stability of the protein without loss of enzymatic activity during each measurement. Typical binding isotherms at 20 °C for the interaction of 2′,5′-ADP with RedΔ40, RedCaM without Ca^{2+}/CaM, and RedCaM with Ca^{2+}/CaM are shown in Figure 6. The data obtained after subtracting the heat of dilution were described by a one-set-of-sites model. As summarized in Table 4, the binding stoichiometry of 2′,5′-ADP was about 1 for all of the reductase proteins, indicating that a single 2′,5′-ADP molecule binds to each nNOS reductase molecule.

The binding affinity of 2′,5′-ADP for RedΔ40 was lower than that for Red, although the kinetically obtained K_a value of NADPH for RedΔ40 was larger than that for Red (Table 1).

Table 4: Thermodynamic Parameters for the Interaction of Red and Its Mutants with 2′,5′-ADP at 20 °C[a]

proteins	n	K_a ($\times 10^4$ M^{-1})	ΔH (kcal·mol^{-1})	ΔG (kcal·mol^{-1})	$T\Delta S$ (kcal·mol^{-1})
Red	1.0	1650 ± 80	−17.2 ± 0.4	−9.7 ± 0.0	−7.5 ± 0.4
RedΔ40	1.3	422 ± 170	−15.8 ± 0.4	−8.9 ± 0.3	−6.9 ± 0.7
RedCaM without CaM	1.3	87.8 ± 9.5	−15.6 ± 0.5	−8.0 ± 0.1	−7.6 ± 0.5
RedCaM with CaM[b]	1.2	588 ± 86	−15.2 ± 0.1	−9.1 ± 0.1	−6.1 ± 0.2

[a]nNOS Red or its mutants and 2′,5′-ADP were dissolved in 100 mM Bes−NaOH buffer, pH 7.0, containing 10% glycerol. All ITC measurements were performed in triplicate at 20°C, and the experimentally determined parameters are shown as the mean and standard deviation. [b]In the case of RedCaM with CaM, the ITC buffer also contained 0.5 mM $CaCl_2$.

Table 5: Comparison of Thermodynamic Parameters for the Interaction of RedCaM with $NADP^+$ in the Absence or Presence of CaM[a]

RedCaM	n	K_a ($\times 10^4$ M^{-1})	ΔH (kcal·mol^{-1})	ΔG (kcal·mol^{-1})	$T\Delta S$ (kcal·mol^{-1})
without CaM					
15 °C	1.2	8.4 ± 4.8	−11.7 ± 3.5	−6.5 ± 0.3	−5.2 ± 3.7
20 °C[b]	1.5	7.3	−10.6	−6.5	−4.1
with CaM					
15 °C	1.3	60.2 ± 7.2	−9.9 ± 0.8	−7.6 ± 0.1	−2.2 ± 0.8
20 °C	1.3	57.7 ± 11.3	−10.5 ± 0.5	−7.7 ± 0.1	−2.8 ± 0.5

[a]The experiments were performed under the same conditions as described in Table 4 except the temperature. [b]Due to the protein instability of RedCaM without CaM during measurements, it was difficult to get data in triplicate at 20 °C.

The $T\Delta S$ values of 2′,5′-ADP binding for Red and RedΔ40 were −7.5 and −6.9 kcal·mol^{-1}, respectively, indicating that the deletion of the AH resulted in a less unfavorable entropy change. However, the binding of 2′,5′-ADP to RedΔ40 showed a large unfavorable ΔH gain (∼1.4 kcal·mol^{-1} difference between Red and RedΔ40) that contributed to the decrease in the K_a value. In the crystal structure of Red, the AH domain was sequestered into a hydrophobic pocket between the NADPH- and FMN-binding domains, repressing electron transfer as shown in Figure 3 (*9*). The deletion of the AH relieves this repression and affects the Ca^{2+}/CaM-dependent activation of electron transfer in NOS (*20*−*24*). Quite recently, Guan et al. (*34*) reported that Lys842 in the AH domain is critical for the known function of AH; in the K842A mutant, NADPH no longer increased the level of FMN shielding, suggesting that AH helps to transduce the effect of NADPH binding on the conformational equilibrium of Red. Therefore, AH might indirectly affect NADPH binding itself. The gain in $T\Delta S$ for binding 2′,5′-ADP to RedΔ40 is consistent with these kinetic results. In addition to the AH, the C-terminal tail affects the stability of the "closed" conformation by directly interacting with the NADPH binding domain. We attempted to determine thermodynamic parameters for the deletion mutant of the CT but could not due to instability of the protein during ITC measurements even under low temperature conditions.

The presence of the CaM binding site also decreased the binding affinity of 2′,5′-ADP (Table 4). In comparison to Red, RedCaM showed an increase in ΔH values independent of Ca^{2+}/CaM addition to the system. The unfavorable gains for RedCaM were 1.6 and 2.0 kcal·mol^{-1} in the absence and presence of Ca^{2+}/CaM, respectively. Recently, Xia and co-workers (*52*) determined the crystal structure of the Ca^{2+}/CaM-bound complex of the isolated CaM and the FMN domain of human iNOS (CaCaM-FMN); the CaM binding site was found to form an α helix extending from the N-terminus of the FMN domain. Although the overall structure of the reductase domain containing the CaM binding site has not been elucidated, this study demonstrated an overlay of the structure of iNOS CaCaM-FMN and the structure of the nNOS reductase domain by superimposing their FMN domains. In the structure, the CaM binding site was located far from the $NADP^+$ binding site, suggesting that the effect of the CaM binding site on cofactor binding was due to the indirect interaction between the two sites.

Ca^{2+}/CaM addition to RedCaM resulted in a 6.7-fold increase in cofactor-binding affinity (from 87.8 to 588 × 10^4 M^{-1}). As shown in Table 4, the $T\Delta S$ values of 2′,5′-ADP binding for RedCaM in the absence and presence of Ca^{2+}/CaM were −7.6 and −6.1 kcal·mol^{-1}, respectively, while the ΔH values were similar. These results indicate that Ca^{2+}/CaM binding to RedCaM resulted in more a favorable entropy change for cofactor binding. Similar results were obtained for the binding of $NADP^+$ to RedCaM as shown in Table 5. The increase of $NADP^+$ binding affinity by Ca^{2+}/CaM was associated with increase of $T\Delta S$ value. 2′,5′-ADP appeared to bind more tightly than $NADP^+$ even in the presence of Ca^{2+}/CaM, suggesting again the importance of the adenosine moiety for the binding. Recently, it was reported that the binding entropy change observed in the total system is linearly correlated to the change in the conformational entropy of the protein (*53*, *54*). Consistent with this previous study, the binding entropic gain of RedCaM indicates that Ca^{2+}/CaM induced the conformational fluctuation of the protein for cofactor binding, although the structure with Ca^{2+}/CaM binding has not been available to date. In consequence, Ca^{2+}/CaM-bound RedCaM could be highly flexible and ready to assume an appropriate conformation (deshielded conformation or open form) for electron transfer in the protein. These data are also consistent with previous kinetic studies showing that Ca^{2+}/CaM binding causes a shift in the conformational equilibrium to more deshielded state and increases electron transfer in the reductase domain and the accessibility of the electron acceptor, such as cytochrome *c*, and the oxygenase domain in the full-length NOS protein (*29*−*31*).

In summary, we have demonstrated the differences in the thermodynamics of cofactor binding between the reductase domain of nNOS (Red) and CPR. $NADP^+$ binding affinity to Red is remarkably lower due to the contribution of an unfavorable, large gain in ΔH relative to that found in CPR. Unlike CPR,

Red distinguishes between 2′,5′-ADP and $NADP^+$, indicating that the nicontinamide moiety of the cofactor is important for interaction with the protein. Binding of cofactors to the deletion mutant of AH (RedΔ40) and to RedCaM in the presence of Ca^{2+}/CaM induces conformational flexibility of the protein. These thermodynamic data provide a structural basis to understand conformational rearrangements induced by cofactor binding for electron transfer in the reductase domain of NOS.

SUPPORTING INFORMATION AVAILABLE

Two figures showing SDS−PAGE and optical absorption spectra of the purified enzymes used for this study. This material is available free of charge via the Internet at http://pubs.acs.org.

REFERENCES

1. Schmidt, H. H., and Walter, U. (1994) NO at work. *Cell 78*, 919–925.
2. Mayer, B., Ed. (2000) *Handb. Exp. Pharmacol.* 143, 206−234.
3. Bredt, D. S., and Snyder, S. H. (1994) Nitric oxide: a physiologic messenger molecule. *Annu. Rev. Biochem. 63*, 175–195.
4. Stuehr, D. J. (1999) Mammalian nitric oxide synthases. *Biochim. Biophys. Acta 1411*, 217–230.
5. Alderton, W. K., Cooper, C. E., and Knowles, R. G. (2001) Nitric oxide synthases: structure, function and inhibition. *Biochem. J. 357*, 593–615.
6. Li, H., and Poulos, T. L. (2005) Structure-function studies on nitric oxide synthases. *J. Inorg. Biochem. 99*, 293–305.
7. Crane, B. R., Arvai, A. S., Ghosh, D. K., Wu, C., Getzoff, E. D., Stuehr, D. J., and Tainer, J. A. (1998) Structure of nitric oxide synthase oxygenase dimer with pterin and substrate. *Science 279*, 2121–2126.
8. Raman, C. S., Li, J., Martásek, P., Kral, V., Masters, B. S. S., and Poulos, T. L. (1998) Crystal structure of constitutive endothelial nitric oxide synthase: a paradigm for pterin function involving a novel metal center. *Cell 95*, 939–950.
9. Garcin, E. D., Bruns, C. M., Lloyd, S. J., Hosfield, D. J., Tiso, M., Gachhui, R., Stuehr, D. J., Tainer, J. A., and Getzoff, E. D. (2004) Structural basis for isozyme-specific regulation of electron transfer in nitric-oxide synthase. *J. Biol. Chem. 279*, 37918–37927.
10. Wang, M., Roberts, D. L., Paschke, R., Shea, T. M., Masters, B. S. S., and Kim, J. J. (1997) Three-dimensional structure of NADPH-cytochrome P450 reductase: prototype for FMN- and FAD-containing enzymes. *Proc. Natl. Acad. Sci. U.S.A. 94*, 8411–8416.
11. Gruez, A., Pignol, D., Zeghouf, M., Coves, J., Fontecave, M., Ferrer, J.-L., and Fontecilla-Camps, J. C. (2000) Four crystal structures of the 60 kDa flavoprotein monomer of the sulfite reductase indicate a disordered flavodoxin-like module. *J. Mol. Biol. 299*, 199–212.
12. Wolthers, K. R., Lou, X., Toogood, H. S., Leys, D., and Scrutton, N. S. (2007) Mechanism of coenzyme binding to human methionine synthase reductase revealed through the crystal structure of the FNR-like module and isothermal titration calorimetry. *Biochemistry 46*, 11833–11844.
13. Siddhanta, U., Presta, A., Fan, B. C., Wolan, D., Rosseau, D. L., and Stuehr, D. J. (1998) Domain swapping in inducible nitric oxide synthase. Electron transfer occurs mainly between flavin and heme groups located on adjacent subunits in the dimmer. *J. Biol. Chem. 273*, 18950–18958.
14. Sagami, I., Daff, S., and Shimizu, T. (2001) Intrasubunit and intersubunit electron transfer in neuronal nitric-oxide synthase: effect of calmodulin on heterodimer catalysis. *J. Biol. Chem. 276*, 30036–30042.
15. Abu-Soud, H. M., Yoho, L. L., and Stuehr, D. J. (1994) Calmodulin controls neuronal nitric-oxide synthase by a dual mechanism. Activation of intra- and interdomain electron transfer. *J. Biol. Chem. 269*, 32047–32050.
16. Matsuda, H., and Iyanagi, T. (1999) Calmodulin activates intramolecular electron transfer between the two flavins of neuronal nitric oxide synthase flavin domain. *Biochim. Biophys. Acta 1473*, 345–355.
17. Salerno, J. C., Harris, D. E., Irizarry., K., Patel, B., Morales, A. J., Smith, S. M. E., Martásek, P., Roman, L. J., Masters, B. S. S., Jones, C. L., Weismann, B. A., Lane, P., Liu, Q., and Gross, S. S. (1997) An autoinhibitory control element defines calcium-regulated isoforms of nitric oxide synthase. *J. Biol. Chem. 272*, 29769–29777.
18. Daff, S., Sagami, I., and Shimizu, T. (1999) The 42-amino acid insert in the FMN domain of neuronal nitric-oxide synthase exerts control over Ca(2+)/calmodulin-dependent electron transfer. *J. Biol. Chem. 274*, 30589–30595.
19. Montgomery, H. J., Romanov, V., and Guillemette, J. G. (2000) Removal of a putative inhibitory element reduces the calcium-dependent calmodulin activation of neuronal nitric-oxide synthase. *J. Biol. Chem. 275*, 5052–5058.
20. Roman, L. J., Martásek, P., Miller, R. T., Harris, D. E., de la Garza, M. A., Shea, T. M., Kim, J.-J. P., and Masters, B. S. S. (2000) The C termini of constitutive nitric-oxide synthases control electron flow through the flavin and heme domains and affect modulation by calmodulin. *J. Biol. Chem. 275*, 29225–29232.
21. Stuehr, D. J., Jesu′ s Tejero, J, and Haque, M. M. (2009) Structural and mechanistic aspects of flavoproteins: electron transfer through the nitric oxide synthase flavoprotein domain. *FEBS J. 276*, 3959–3974.
22. Welland, A, Garnaud, P. E., Kitamura, M, Miles, C. S., and Daff, S. (2008) Importance of the domain-domain interface to the catalytic action of the NO synthase reductase domain. *Biochemistry 47*, 9771–9780.
23. Fulton, D., Gratton, J. P., McCabe, T. J, Fontana, J., Fujio, Y., Walsh, K., Franke, T. F., Papapetropoulos, A., and Sessa, W. C. (1999) Regulation of endothelium-derived nitric oxide production by the protein kinase Akt. *Nature 399*, 597–601.
24. Adak, S., Santolini, J., Tikunova, S., Wang, Q., Johnson, J. D., and Stuehr, D. J. (2001) Neuronal nitric-oxide synthase mutant (Ser-1412 → Asp) demonstrates surprising connections between heme reduction, NO complex formation, and catalysis. *J. Biol. Chem. 276*, 1244–1252.
25. Tran, Q. K., Leonard, J., Black, D. J., and Persechini, A. (2008) Phosphorylation within an autoinhibitory domain in endothelial nitric oxide synthase reduces the Ca^{2+} concentrations required for calmodulin to bind and activate the enzyme. *Biochemistry 47*, 7557–7566.
26. Daff, S., Noble, M. A., Craig, D. H., Rivers, S. L., Chapman, S. K., Munro, A. W., Fujiwara, S., Rozhkova, E., Sagami, I., and Shimizu, T. (2001) Control of electron transfer in neuronal NO synthase. *Biochem. Soc. Trans. 29*, 147–152.
27. Craig, D. H., Chapman, S. K., and Daff, S. (2002) Calmodulin activates electron transfer through neuronal nitric-oxide synthase reductase domain by releasing an NADPH-dependent conformational lock. *J. Biol. Chem. 277*, 33987–33994.
28. Adak, S., Sharma, M., Meade, A. L., and Stuehr, D. J. (2002) A conserved flavin-shielding residue regulates NO synthase electron transfer and nicotinamide coenzyme specificity. *Proc. Natl. Acad. Sci. U.S.A. 99*, 13516–13521.
29. Konas, D. W., Zhu, K., Sharma, M., Aulak, K. S., Brudvig, G. W., and Stuehr, D. J. (2004) The FAD-shielding residue Phe1395 regulates neuronal nitric-oxide synthase catalysis by controlling $NADP^+$ affinity and a conformational equilibrium within the flavoprotein domain. *J. Biol. Chem. 279*, 35412–35425.
30. Jachymova, M., Martásek, P., Panda, S., Roman, L. J., Panda, M., Shea, T. M., Ishimura, Y., Kim, J.-J. P., and Masters, B. S. S. (2005) Recruitment of governing elements for electron transfer in the nitric oxide synthase family. *Proc. Natl. Acad. Sci. U.S.A. 102*, 15833–15838.
31. Tiso, M., Konas, D. W., Panda, K., Garcin, E. D., Sharma, M., Getzoff, E. D., and Stuehr, D. J. (2005) C-terminal tail residue Arg1400 enables NADPH to regulate electron transfer in neuronal nitric-oxide synthase. *J. Biol. Chem. 280*, 39208–39219.
32. Tiso, M., Tejero, J., Panda, K., Aulak, K. S., and Stuehr, D. J. (2007) Versatile regulation of neuronal nitric oxide synthase by specific regions of its C-terminal tail. *Biochemistry 46*, 14418–14428.
33. Ilagan, R. P., Tejero, J., Aulak, K. S., Ray, S. S., Hemann, C., Wang, Z. Q., Gangoda, M., Zweier, J. L., and Stuehr, D. J. (2009) Regulation of FMN subdomain interactions and function in neuronal nitric oxide synthase. *Biochemistry 48*, 3864–3876.
34. Guan, Z. W., Haque, M. M., Wei, C. C, Garcin, E. D., Getzoff, E. D., and Stuehr, D. J. (2010) Lys842 in neuronal nitric-oxide synthase enables the autoinhibitory insert to antagonize calmodulin binding, increase FMN shielding, and suppress interflavin electron transfer. *J. Biol. Chem. 285*, 3064–3075.
35. Knight, K., and Scrutton, N. S. (2002) Stopped-flow kinetic studies of electron transfer in the reductase domain of neuronal nitric oxide synthase: reevaluation of the kinetic mechanism reveals new enzyme intermediates and variation with cytochrome P450 reductase. *Biochem. J. 367*, 19–30.
36. Daff, S. (2004) An appraisal of multiple NADPH binding-site models proposed for cytochrome P450 reductase, NO synthase, and related diflavin reductase systems. *Biochemistry 43*, 3929–3932.

37. Grunau, A, Paine, M. J., Ladbury, J. E., and Gutierrez, A. (2006) Global effects of the energetics of coenzyme binding: NADPH controls the protein interaction properties of human cytochrome P450 reductase. *Biochemistry 45*, 1421–1434.
38. Sato, Y., Sagami, I., and Shimizu, T. (2004) Identification of caveolin-1-interacting sites in neuronal nitric-oxide synthase. Molecular mechanism for inhibition of NO formation. *J. Biol. Chem. 279*, 8827–8836.
39. Rozhkova, E. A., Fujimoto, N., Sagami, I., Daff, S. N., and Shimizu, T. (2002) Interactions between the isolated oxygenase and reductase domains of neuronal nitric-oxide synthase: assessing the role of calmodulin. *J. Biol. Chem. 277*, 16888–16894.
40. Goloubinoff, P., Gatenby, A. A., and Lorimer, G. H. (1989) GroE heat-shock proteins promote assembly of foreign prokaryotic ribulose bisphosphate carboxylase oligomers in *Escherichia coli*. *Nature 337*, 44–47.
41. Gutierrez, A., Lian, L. Y., Wolf, C. R., Scrutton, N. S., and Roberts, G. C. (2001) Stopped-flow kinetic studies of flavin reduction in human cytochrome P450 reductase and its component domains. *Biochemistry 40*, 1964–1975.
42. Roitel, O., Scrutton, N. S., and Munro, A. W. (2003) Electron transfer in flavocytochrome P450 BM3: kinetics of flavin reduction and oxidation, the role of cysteine 999, and relationships with mammalian cytochrome P450 reductase. *Biochemistry 42*, 10809–10821.
43. Wolthers, K. R., and Schimerlik, M. I. (2001) Reaction of neuronal nitric-oxide synthase with 2,6-dichloroindolphenol and cytochrome c^{3+}: influence of the electron acceptor and binding of Ca^{2+}-activated calmodulin on the kinetic mechanism. *Biochemstry 40*, 4722–4737.
44. Dunford, A. J., Rigby, S. E., Hay, S., Munro, A. W., and Scrutton, N. S. (2007) Conformational and thermodynamic control of electron transfer in neuronal nitric oxide synthase. *Biochemistry 46*, 5018–5029.
45. Lumry, R. (2003) Uses of enthalpy-entropy compensation in protein research. *Biophys. Chem. 105*, 545–557.
46. Sturtevant, J. M. (1977) Heat capacity and entropy changes in processes involving proteins. *Proc. Natl. Acad. Sci. U.S.A. 74*, 2236–2240.
47. Luque, I., Todd, M. J., Gomez, J., Semo, N., and Freire, E. (1998) Molecular basis of resistance to HIV-1 protease inhibition: a plausible hypothesis. *Biochemistry 37*, 5791–5797.
48. Spolar, R. S., and Record, M. T., Jr. (1994) Coupling of local folding to site-specific binding of proteins to DNA. *Science 263*, 777–784.
49. Gomez, J., Hilser, V. J., Xie, D., and Freire, E. (1995) The heat capacity of proteins. *Proteins 22*, 404–412.
50. Bergqvist, S., Williams, M. A., O'Brien, R., and Ladbury, J. E. (2004) Heat capacity effects of water molecules and ions at a protein-DNA interface. *J. Mol. Biol. 4*, 829–842.
51. Grunau, A., Geraki, K., Grossmann, J. G, and Gutierrez, A. (2007) Conformational dynamics and the energetics of protein-ligand interactions: role of interdomain loop in human cytochrome P450 reductase. *Biochemistry 46*, 8244–8255.
52. Xia, C., Misra, I., Iyanagi, T., and Kim, J.-J. P. (2009) Regulation of interdomain interactions by calmodulin in inducible nitric-oxide synthase. *J. Biol. Chem. 284*, 30708–30717.
53. Frederick, K. K., Marlow, M. S., Valentine, K. G., and Wand, A. J. (2007) Heat capacity and entropy changes in processes involving proteins. *Nature 448*, 325–329.
54. Marlow, M. S., Dogan, J., Frederick, K. K., Valentine, K. G., and Wand, A. J. (2010) The role of conformational entropy in molecular recognition by calmodulin. *Nat. Chem. Biol. 6*, 352–358.